J|A|C|S
ARTICLES

Published on Web 07/21/2009

A Realistic Description of the Charge Carrier Wave Function in Microcrystalline Polymer Semiconductors

D. L. Cheung, D. P. McMahon, and A. Troisi*

Department of Chemistry and Centre of Scientific Computing, University of Warwick, CV4 7AL Coventry, U.K.

Received May 12, 2009; E-mail: a.troisi@warwick.ac.uk

Abstract: The electronic structure of the charge carrier in one of the most commonly used semiconducting polymers (poly(3-hexylthiophene (P3HT)) is described using a combination of classical and quantum chemical methods. It is shown that the carriers are localized in correspondence with long-lived traps which are present also in the crystalline phase of the polymer. The existence of activated transport for very ordered polymer phases (regardless of the strength of the polaron formation energy) is explained, and the trapped states, postulated by many phenomenological models, are described for the first time with chemical detail. It is shown that computational chemistry methods can be used to fill the gap between phenomenological descriptions of charge transport in polymers and microscopic descriptions of the individual quantum dynamic processes.

Introduction

The potential uses of polymer semiconductors for disparate electronics applications requiring inexpensive and flexible materials has attracted the interest of many researchers and transformed their study into one of the most active areas of material science. The growth of this research field, catalyzed by the successful realization of polymer light-emitting diodes,[1,2] and the promising performance of the currently available polymer thin-film transistors[3−5] and photovoltaic cells,[6,7] was accompanied by a joint effort by scientists with different backgrounds to understand the fundamental properties of these materials. Therefore, it might be surprising that a relation between the chemical composition of the material and the charge mobility (the most important characteristic for an organic semiconductor) is not known, and even the qualitative models used to describe charge transport are actively debated.[8−10] This lack of a structure−property relationship is particularly penalizing for a field which built its promise on the ability of synthetic polymer chemistry to tailor-make materials for electronics.

Only for molecular crystals,[11,12] perfectly crystalline polymers,[13] and some liquid crystal[14] is it possible to compute from first principles the basic parameters that determine the charge transport. The situation is more complicated for disordered or partially ordered polymers, whose transport is described with a set of methods originating from the physics of disordered systems.[15] It is commonly assumed that the disorder of the material will produce low-energy localized states which will be occupied by the charge carrier. The localized charge can hop to another localized state with a rate that depends on the energy difference between the two states and the distance between them. The large number of models based on this idea go under the name of variable range hopping (VRH) models. They differ in their assumption on the type of density of states (DOS) distribution (Gaussian[16] or exponential[17]), the rate to be used for the hopping (e.g., Marcus[18] or Miller-Abrahams[19]), the possible correlation between site energies,[20] and the methods to be used to extract the mobility of the material (analytical[21,22] or numerical[16]). As these methods are invariably characterized by a number of parameters, which are fitted to the experimental

(1) Burroughes, J. H.; Bradley, D. D. C.; Brown, A. R.; Marks, R. N.; Mackay, K.; Friend, R. H.; Burns, P. L.; Holmes, A. B. *Nature* **1990**, *347*, 539.
(2) Sheats, J. R.; Antoniadis, H.; Hueschen, M.; Leonard, W.; Miller, J.; Moon, R.; Roitman, D.; Stocking, A. *Science* **1996**, *273*, 884.
(3) Burroughes, J. H.; Jones, C. A.; Friend, R. H. *Nature* **1988**, *335*, 137.
(4) Horowitz, G.; Fichou, D.; Peng, X. Z.; Xu, Z. G.; Garnier, F. *Solid State Commun.* **1989**, *72*, 381.
(5) Sirringhaus, H. *Adv. Mater.* **2005**, *17*, 2411.
(6) Granstrom, M.; Petritsch, K.; Arias, A. C.; Lux, A.; Andersson, M. R.; Friend, R. H. *Nature* **1998**, *395*, 257.
(7) Peumans, P.; Uchida, S.; Forrest, S. R. *Nature* **2003**, *425*, 158.
(8) Coropceanu, V.; Cornil, J.; da Silva, D. A.; Olivier, Y.; Silbey, R.; Bredas, J. L. *Chem. Rev.* **2007**, *107*, 926.
(9) Grozema, F. C.; Siebbeles, L. D. A. *Int. Rev. Phys. Chem.* **2008**, *27*, 87.
(10) Cheung, D. L.; Troisi, A. *Phys. Chem. Chem. Phys.* **2008**, *10*, 5941.
(11) Cheng, Y. C.; Silbey, R. J.; da Silva Filho, D. A.; Calbert, J. P.; Cornil, J.; Bredas, J. L. *J. Chem. Phys.* **2003**, *118*, 3764.
(12) Troisi, A. *Adv. Mater.* **2007**, *19*, 2000.
(13) Dacosta, P. G.; Dandrea, R. G.; Conwell, E. M. *Phys. Rev. B* **1993**, *47*, 1800.
(14) Kirkpatrick, J.; Marcon, V.; Nelson, J.; Kremer, K.; Andrienko, D. *Phys. Rev. Lett.* **2007**, *98*, 227402.
(15) Baranovski, S. E. *Charge Transport in Disordered Solids with Applications in Electronics*; Wiley: West Sussex, 2006.
(16) Bassler, H. *Phys. Status Solidi B* **1993**, *175*, 15.
(17) Street, R. A.; Northrup, J. E.; Salleo, A. *Phys. Rev. B* **2005**, *71*, 165202.
(18) Marcus, R. *J. Chem. Phys.* **1956**, *24*, 966.
(19) Miller, A.; Abrahams, B. *Phys. Rev. B* **1960**, *120*, 745.
(20) Novikov, S. V.; Dunlap, D. H.; Kenkre, V. M.; Parris, P. E.; Vannikov, A. V. *Phys. Rev. Lett.* **1998**, *81*, 4472.
(21) Cordes, H.; Baranovskii, S. D.; Kohary, K.; Thomas, P.; Yamasaki, S.; Hensel, F.; Wendorff, J. H. *Phys. Rev. B* **2001**, *6309*, 094201.
(22) Coehoorn, R.; Pasveer, W. F.; Bobbert, P. A.; Michels, M. A. J. *Phys. Rev. B* **2005**, *72*, 155206.

10.1021/ja903843c CCC: $40.75

mobility as a function of the carrier concentration and temperature, they do not provide any kind of structure property relation even when the fitting with the experimental data is fully satisfactory. Alternative phenomenological methods based on percolation theory[23] or mobility edge models[24] suffer from similar drawbacks.

The limitation of phenomenological modeling is particularly evident when we consider probably the most studied semiconducting polymer, poly(3-hexylthiophene) (P3HT),[25,26] which displays a microcrystalline phase with very long-range ordering along and between polymeric chains. It is very difficult to conciliate the assumption of a completely disordered phase with the crystallographic experimental evidence: the system is closer to an ordered system (with some defects) than to a disordered system (possibly with some correlation). Moreover, several studies have shown that an increase in crystalline order[27,28] in P3HT is associated with an increase in mobility, and these observations are difficult to explain if we assume the presence of a disordered phase to begin with. Experimental evidence points unambiguously toward the presence of trapped localized states as the transport is always thermally activated. It is therefore essential to understand what the 'chemical' nature of the traps is in order to build the most appropriate transport model 'from the bottom-up'. For example, if the wave function of the localized states is known, one can use chemical charge transfer theories[29] to describe the hopping of the charge between two localized states.

In this paper we will describe the wave function of the charge carrier (hole) for P3HT (the most studied of the semiconducting polymers) using a combination of molecular dynamics (MD) simulations on an atomistic model of the polymer and semiempirical quantum chemistry computations. This combination of methods[30] proved particularly useful for the study of semiconducting molecular crystals[31,32] and liquid crystals[14] and it provides a natural way to adapt the descriptions based on model Hamiltonians[33−35] to realistic materials. Through the characterization of the low-energy states occupied by the charge carrier in a realistic model of the polymer, this work aims to act as a bridge between the description of the global properties of the material (covered by the phenomenological models) and the description of the individual charge transfer process (covered by condensed phase quantum dynamics). As we will see, this work will also provide an interesting link between disorder-based models and polaron theories[36] which have traditionally been more successful when applied to molecular crystals. After describing, in the next section, the details of our classical simulations, we will present the result of the quantum chemical computations, their analysis, and a discussion of the significance of our results.

Molecular Dynamics. The simulated system contained 12 chains of regioregular-P3HT, each consisting of 40 thiophene rings, arranged in two layers of six chains. Initially, the distance between the chains was 3.8 Å perpendicular to the rings (taken to be the *x*-direction) and 16 Å parallel to the rings (*y*-direction). The side chains were fully extended and interdigitated. This structure corresponds to the so-called type-II polymorph of the polyalkylthiophenes,[37,38] which is the expected structure for low-molecular-mass samples (as studied in this work). Polyalkylthiophenes also exhibit a second polymorph (type-I) with tilted rather than interdigitated side chains.[39,40] Type-II regions are also commonly found as minority components in high-molecular-mass samples, predominantly consisting of type-I regions.[41,42] The length of the polymer chains (∼160 Å) is significantly smaller than the typical hopping range considered by VRH models.[15]

The force field used in this work has been previously employed and validated on studies of various thiophene systems,[43,44] including poly(3-butylthiophene),[45] which is closely related to P3HT studied in this work. Bond stretching and bond angle bending are described by harmonic potentials, with identical equilibrium bond lengths, angles and force constants given by the leading (harmonic) term in the MM3 potentials. Cross-terms (e.g., stretch−bend, stretch−stretch terms) are neglected. Nonbonded parameters were taken from the OPLS parameter set,[46] along with the torsional parameters for the alkyl chains. The torsional potential between the thiophene rings was found from *ab initio* calculations (MP2/aug-cc-pVTZ) on 2-2′-bithiophene.[47] In order to assess the suitability of this torsional potential for the presented system, the torsional potential for 2-2′-dimethylthiophene has been calculated from the force field and from *ab initio* (MP2/6-31G*) calculations. As shown in the Supporting Information (Figure S2) the force field potential provides a good representation of the *ab initio* potential, in particular the potential minima in the force field potential coincide with those in the *ab initio*. Full details of the force field, including an explicit listing of the force field parameters, may be found in the Supporting Information. Simulations were performed using the DL_POLY program.[48] Equations of motion are integrated using the velocity Verlet integrator, with time step of 1 fs, and harmonic bonds were constrained using the SHAKE algorithm. The presence of high-frequency bond

(23) Vissenberg, M.; Matters, M. *Phys. Rev. B* **1998**, *57*, 12964.
(24) Salleo, A.; Chen, T. W.; Volkel, A. R.; Wu, Y.; Liu, P.; Ong, B. S.; Street, R. A. *Phys. Rev. B* **2004**, *70*, 115311.
(25) Bao, Z.; Dodabalapur, A.; Lovinger, A. J. *Appl. Phys. Lett.* **1996**, *69*, 4108.
(26) McCullough, R. D. *Adv. Mater.* **1998**, *10*, 93.
(27) Yang, H. C.; Shin, T. J.; Yang, L.; Cho, K.; Ryu, C. Y.; Bao, Z. N. *Adv. Funct. Mater.* **2005**, *15*, 671.
(28) Jimison, L. H.; Salleo, A.; Chabinyc, M. L.; Bernstein, D. P.; Toney, M. F. *Phys. Rev. B* **2008**, *78*, 125319.
(29) Nitzan, A. *Chemical Dynamics in Condensed Phases*; Oxford University Press: New York, 2006.
(30) Vukmirovic, N.; Wang, L. W. *J. Phys. Chem. B* **2009**, *113*, 409.
(31) Troisi, A.; Orlandi, G. *J. Phys. Chem. A* **2006**, *110*, 4065.
(32) Troisi, A.; Orlandi, G.; Anthony, J. E. *Chem. Mater.* **2005**, *17*, 5024.
(33) Hultell, M.; Stafstrom, S. *Phys. Rev. B* **2007**, *75*, 104304.
(34) Prins, P.; Grozema, F. C.; Galbrecht, F.; Scherf, U.; Siebbeles, L. D. A. *J. Phys. Chem. C* **2007**, *111*, 11104.
(35) Troisi, A.; Orlandi, G. *Phys. Rev. Lett.* **2006**, *96*, 086601.
(36) Geskin, V. M.; Dkhissi, A.; Bredas, J. L. *Int. J. Quantum Chem.* **2003**, *91*, 350.
(37) Prosa, T. J.; Winokur, M. J.; McCullough, R. D. *Macromolecules* **1996**, *29*, 3654.
(38) Joshi, S.; Grigorian, S.; Pietsch, U. *Phys. Status Solidi A* **2008**, *205*, 488.
(39) Prosa, T. J.; Winokur, M. J.; Moulton, J.; Smith, P.; Heeger, A. J. *Macromolecules* **1992**, *25*, 4364.
(40) Kline, R. J.; DeLongchamp, D. M.; Fischer, D. A.; Lin, E. K.; Richter, L. J.; Chabinyc, M. L.; Toney, M. F.; Heeney, M.; McCulloch, I. *Macromolecules* **2007**, *40*, 7960.
(41) Meille, S. V.; Romita, V.; Caronna, T.; Lovinger, A. J.; Catellani, M.; Belobrzeckaja, L. *Macromolecules* **1997**, *30*, 7898.
(42) Prosa, T. J.; Moulton, J.; Heeger, A. J.; Winokur, M. J. *Macromolecules* **1999**, *32*, 4000.
(43) Marcon, V.; Raos, G. *J. Am. Chem. Soc.* **2006**, *128*, 1408.
(44) Marcon, V.; Raos, G.; Campione, M.; Sassella, A. *Cryst. Growth Des.* **2006**, *6*, 1826.
(45) Arosio, P.; Moreno, M.; Famulari, A.; Raos, G.; Catellani, M.; Meille, S. V. *Chem. Mater.* **2009**, *21*, 78.
(46) Jorgensen, W. L.; Maxwell, D. S.; TiradoRives, J. *J. Am. Chem. Soc.* **1996**, *118*, 11225.
(47) Marcon, V.; Raos, G. *J. Phys. Chem. B* **2004**, *108*, 18053.
(48) Smith, W.; Todorov, I. T. *Mol. Simul.* **2006**, *32*, 935.

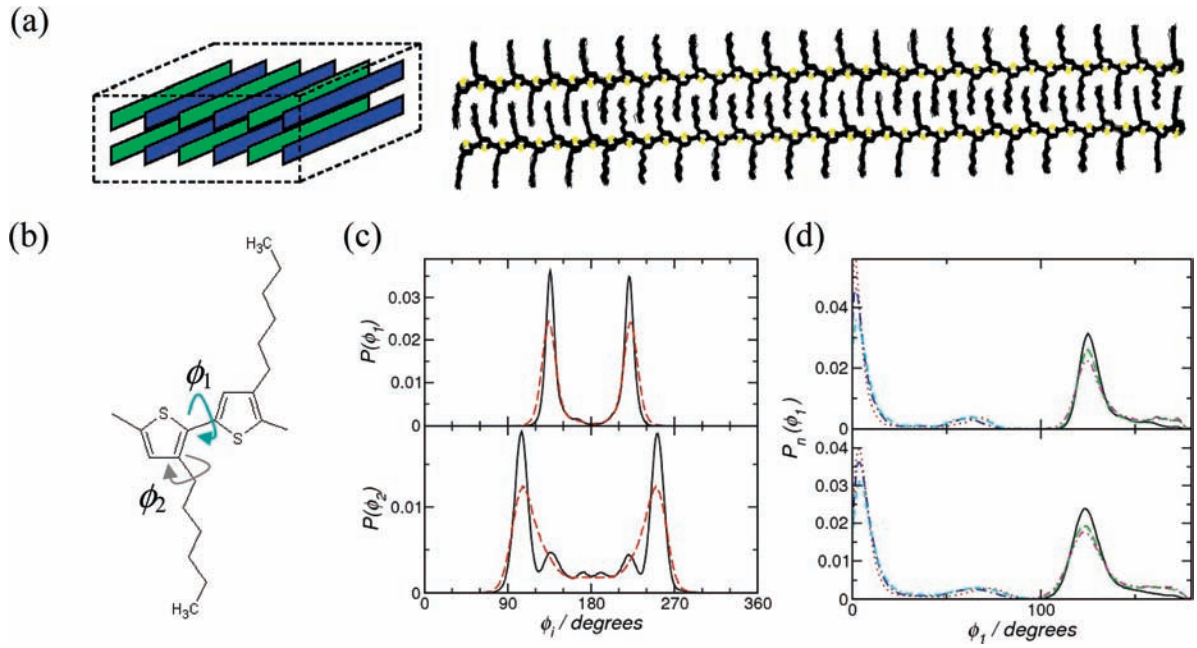

Figure 1. (a) Schematic diagram (left) and representative simulation snapshot (at 300 K) (right). (b) Structure of a P3HT dimer, showing dihedral angles ϕ_1 and ϕ_2. (c) Dihedral angle probability distribution functions at 100 K (solid) and 300 K (dashed) for ϕ_1 (top) and ϕ_2 bottom. (d) Dihedral angle probability distribution function $P_n(\phi_1)$ (defined in text). Solid line (black) denotes $n = 0$, dotted line (red) $n = 1$, dashed line (green) $n = 2$, dot-dashed line (blue) $n = 3$, double-dot-dashed line (cyan) $n = 4$, and dot-double-dashed line (magenta) $n = 5$.

stretches (both C−H bonds and strong C−C double bonds within the thiophene rings) would necessitate the use of a significantly shorter time step (0.2−0.5 fs) in the absence of bond constraints, and the effect on the structure (hence, electronic properties) from bond length changes is likely to be small compared to conformational changes due to dihedral rotations. The simulations were performed in the constant-NPT ensemble, using the Nose−Hoover thermostat and anisotropic barostat[49] (with relaxation times of 0.1 and 0.5 ps, respectively) with long-range electrostatics evaluated using a smooth particle mesh Ewald (SPME) sum[50] with a convergence parameter of 0.32 $Å^{-1}$ and 16, 16, and 40 wavevectors in *x*-, *y*-, *z*-directions.

Considering that the observed mobility is ∼0.1 $cm^2\ s^{-1}\ V^{-1}$, it is possible to estimate that the expected hole permanence time on a segment of ∼5 monomers is about 10−100 ps. Contrary to many polymer physics applications we are therefore not interested in the study of long trajectories; instead, we preferred to run many independent MD trajectories of the order 0.1−1 ns length to get a better averaging over the initial configurations. These configurations were generated using an annealing protocol consisting of successive heating−cooling cycles. Configurations originally run at 100 K (two independent starting configurations were used) were heated up to 300 K (by assigning new velocities from a Maxwell−Boltzmann distribution). These were simulated for 800 ps and split into 500 ps of equilibration and 300 ps of production (data gathering). The final configurations from these were then cooled to 100 K and simulated for a further 800 ps. After two cycles for each of the starting configurations, a run at 400 K was performed, after which two more cycles were performed. Results of 9 simulations at each temperature of 100 and 300 K are presented here and used in the subsequent analysis. A representative simulation configuration, taken at 300 K, is shown in Figure 1a. At this temperature the polymer backbones remain well ordered, while there is a modest degree of disorder in the side chains. Simulations at higher temperatures show that the backbones remain ordered above 400 K. Side chains are interdigitated (see Figure 1a), as commonly found in low-molecular-weight samples,[38] but non-interdigitated crystalline phases have also been reported.[40] The polymer backbones remain well ordered in the temperature range considered here (100−400 K), while there is a modest degree of disorder in the side chains.

The conformational disorder may be studied quantitatively through the dihedral angle probability distributions, shown in Figure 1c. At both 100 and 300 K the inter-ring dihedral (ϕ_1) shows two peaks (of roughly equal height) at about 130° and 230°. This indicates that, as expected, there is typically an approximately 50° dihedral angle between neighboring rings. These peaks are more diffuse at 300 K, due to increased thermal motion. Long-range correlations exist between the orientations of non-neighboring rings. These correlations are shown by the probability distribution function $P_n(\phi)$ (Figure 1d), which gives the probability of two rings separated by n neighbors having an angle of ϕ. An alternating arrangement of ring orientations along the polymer backbone is clearly seen, with an angle of approximately 50° between nearest neighbor rings, while next-nearest neighboring rings lie approximately planar, a pattern which continues along the length of the polymer chains.

The side-chain torsion (dihedral angle ϕ_2) shows larger variations with temperature. At 100 K there are well-defined peaks at approximately 100° and 260°, with a number of smaller peaks in the distribution between these two. At 300 K, the peaks at 100° and 260° are more diffuse whereas between these peaks the distribution is more uniform, indicating a larger degree of disorder in the side-chain orientations. While the side chains are expected to have little direct impact on the charge transfer, the strong coupling between the inter-ring and side-chain torsions, due to packing constraints, means that these will have

(49) Melchionna, S.; Ciccotti, G.; Holian, B. L. *Mol. Phys.* **1993**, *78*, 533.
(50) Essmann, U.; Perera, L.; Berkowitz, M. L.; Darden, T.; Lee, H.; Pedersen, L. G. *J. Chem. Phys.* **1995**, *103*, 8577.

an indirect influence on the intrachain charge transfer, as we will see in the next section. Disruption to the molecular packing due to side-chain disorder is also likely to influence the interchain charge transfer (not considered in this work). In this paper we limited the analysis of the MD trajectory to those aspects affecting the nature of the charge carrier in P3HT (the topic of this work), while additional analysis of the structure and thermodynamic parameters will be presented elsewhere.

The Wave Function of the Hole: Static Localization. To characterize the nature of the electron/hole in P3HT we computed the molecular orbitals (MOs) of all the individual chains in the system for many snapshots of the MD simulations. Only the conjugated backbone was included in the quantum chemical computations (the alkyl side chains were removed and the dangling bonds saturated with hydrogen). Here, we present results obtained with the AM1 semiempirical method[51] (we have verified that the results for other semiempirical methods, such as CNDO, are very similar and the main findings of this work are also confirmed by a smaller set of DFT computations). We are interested in the general localization features of the MOs along the polymer chain and, for this reason, we will consider the orbital density per monomer. For any MO k, this is defined as

$$D_{n,k} = \sum_j \left| C_{j,k} \right|^2$$

where the summation runs on all atomic orbitals j localized on the monomer n and $C_{j,k}$ are the MO coefficients from the quantum chemical computation (the atomic basis set is considered orthonormal in the AM1 approximation). The average position of the density $D_{n,k}$ for orbital k (expectation value of the position operator) was computed as

$$<n_k> = \sum_n n D_{n,k}$$

and we defined the *localization length* as 2 times the standard deviation σ_k of the orbital density

$$\sigma_k^2 = \sum_n n^2 D_{n,k} - <n>_k^2$$

For each considered trajectory, snapshots were analyzed every 1 ps with the MOs computed on each chain of the simulation. We will mostly consider the features of the HOMO orbital (which describes the positive charge or hole) as P3HT is mostly studied as a p-type semiconductor.

As thermal fluctuations break the translational symmetry of the polymer chain, it is expected that the polymer MOs become localized by dynamic disorder in analogy to what happens for molecular crystals[35] and is illustrated in Figure 2 for P3HT (it is well-known that any amount of disorder causes localization in one-dimensional periodic systems[52]). In our case, however, a more dramatic effect is observed: there are polymer chains for which the HOMO of the chain (the most stable state for the charge carrier) is persistently localized on one site for the length of the simulation (up to 5 ns). As the charge diffusion along the chain is known to be much faster than the simulation length, the persistently localized states behave as if due to static disorder. To make our analysis more quantitative we classified the HOMO wave function as either *strongly localized* or *weakly localized*, on average, along the analyzed trajectory. We define

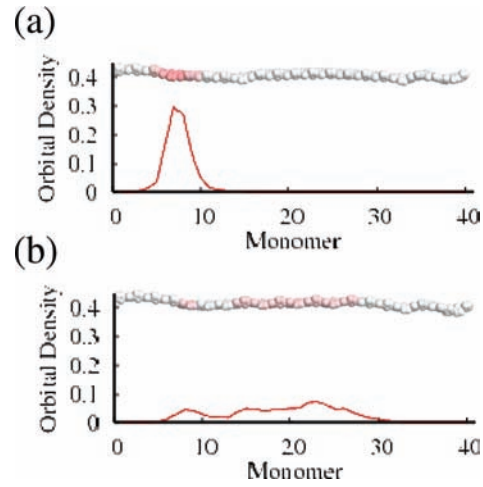

Figure 2. Example orbital density profiles for the HOMO along a single polymer chain (D_{nk} in the text) for one particular snapshot for a strongly (a) and weakly (b) localized case. The inset shows the conformation of the chain used for these calculations (in a color scale where the more intense red color corresponds to higher orbital density).

the wave function as strongly localized if the average of the orbital density localization lengths (taken as twice the standard deviation of the orbital density localization position) over the duration of the simulation is less than four monomer units. The wave function was also categorized according to its time dependence as being *persistent* on one site for the analyzed trajectory of 300 ps or *nonpersistent* (i.e., the localized HOMO is located in different places in consecutive snapshots, an example of *dynamic localization*). In the case of persistent localization we also observed several instances where the HOMO is localized preferentially in two (or three) fixed locations during the simulation (referred to as double (or triple) persistence). These cases can be clearly identified by plotting the orbital density profile along the chain versus time, as done in Figure 3. For the statistical analysis of the results we classified the orbital density as persistently localized if, over the course of a simulation run, the mean position of orbital density localization was found to remain over a region of four consecutive monomers for over 80% of the time (an analogous criterion is used for double and triple persistence).

Table 1 details the fraction of chains exhibiting the different localization characteristics for the orbitals HOMO−1, HOMO, and LUMO as found in all the simulations presented in this work. It is found that approximately 28% of the chains of the simulations at 300 K show static disorder, leading to the localization of the HOMO density at a single site. A further 17% show localization at multiple positions. The HOMO−1 orbital density is found to be weakly localized for all simulations. In contrast, the HOMO and LUMO both show strong localization of the orbital density approximately 30% of the time, with the localization being greatest when it is persistent over the course of the simulation. Although this combined molecular simulation/quantum chemical approach cannot provide a very accurate estimate of the concentration of each individual type of trap, from the available data, we can estimate the presence of a persistently localized state every ∼60 monomers at 300 K. We should also mention that the equilibrium bond distances of the AM1 Hamiltonian are slightly different than those of the used force field, although the difference is typically less than 1%. We verified that this mismatch between the quantum and classical methods does not affect the main results of this paper

(51) Dewar, M. J. S.; Zoebisch, E. G.; Healy, E. F.; Stewart, J. J. P. *J. Am. Chem. Soc.* **1985**, *107*, 3902.
(52) Lee, P. A.; Ramakrishnan, T. V. *Rev. Mod. Phys.* **1985**, *57*, 287.

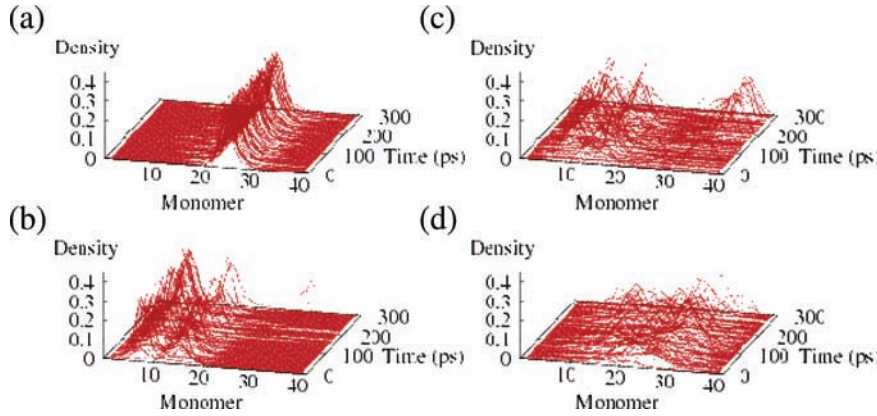

Figure 3. HOMO density profile during the course of the simulation. They are classified according to the persistence of the localized state during the simulation as single persistent (a), double persistent (b), triple persistent, (c) or nonpersistent (d).

Table 1. Localization Type and Persistence Type of the Orbital Density for Individual Polymer Chains over the Course of the Analyzed Trajectories at 100 and 300 K

		localization type		persistence type			
T (K)	orbital	strong (%)	weak (%)	single (%)	double (%)	triple (%)	nonpersistent (%)
100	HOMO−1	0	100	0	8	17	75
	HOMO	30	70	38	22	12	28
	LUMO	26	74	42	15	13	30
300	HOMO−1	0	100	0	0	2	98
	HOMO	31	69	28	11	6	55
	LUMO	29	71	26	11	14	49

(existence and nature of the localized states) by recomputing the HOMO for uncorrelated chains after reoptimizing the bond length at the AM1 level. We observed that the orbital density profile is effectively unchanged by the bond optimization and the orbital energy is systematically shifted upward by ∼0.2 eV.

It was also observed that, in the case of strong localization, the LUMO is generally localized where the HOMO is localized so that the lowest-energy optical transitions will likely involve these two localized orbitals. We reported in Figure 4 the distribution of $|\langle n\rangle_{\mathrm{HOMO}} - \langle n\rangle_{\mathrm{LUMO}}|$ (the difference between the localization position of the HOMO and LUMO orbitals) distinguishing the cases of strongly localized (with single persistence) and weakly localized HOMO. We found that, when the HOMO is strongly localized, the LUMO is within 1 to 2 monomers of it, while for weaker localization, there is a much weaker tendency for the LUMO to be close to the HOMO. This feature is also important because the possibility that the charge hopping paths are similar for hole and electron influences the modeling of charge recombination in photovoltaic devices.[53]

The most relevant case is that of a persistently localized HOMO because these are the most likely to be occupied by the holes at low carrier density. These localized states are due to a new distorted minimum in the potential energy surface, and unlike the dynamic localization found in molecular crystals, they are not due to large amplitude oscillations about an equilibrium position. It is therefore interesting to analyze the conformation of the polymer where the HOMO is localized to describe the 'chemical origin' of the localization. We found that, in the majority of cases of persistently localized HOMOs, there is a substantial deviation in the inter-ring dihedral angle (ϕ_1) away from the average value of ±50° and toward planarity (0°), as

(53) Rappaport, N.; Solomesch, O.; Tessler, N. *J. Appl. Phys.* **2006**, *99*, 064507.

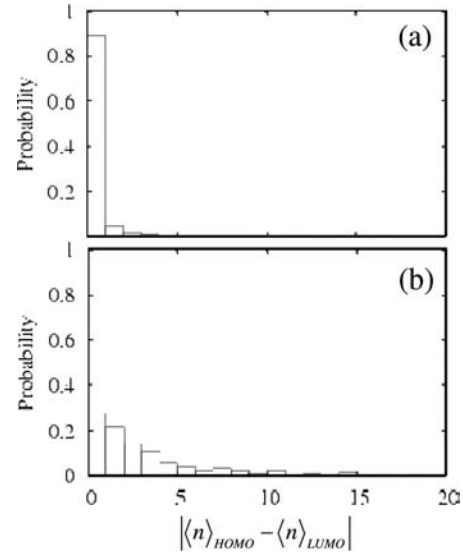

Figure 4. Probability distribution for the absolute difference in the position of the HOMO and LUMO in the case of strongly (a) and weakly (b) localized HOMO over the course of a 300 ps simulation at 300 K.

exemplified by the case shown in Figure 5. In 80% of cases with persistent localization, in correspondence with the localized HOMO, one of the inter-ring dihedral angles is less than 20°; in 65% of the cases the side-chain torsion angle (ϕ_2) also shows a deviation of more than 60° with respect to the equilibrium value. In other words, the localized states are due to a locally planarized structure of the P3HT chain which is also illustrated in Figure 5. This locally planar structure is kept out of equilibrium by the steric interaction with the other chains so that, *even though the alkyl chains do not contribute to the electronic structure of the HOMO, they determine the deformation which causes the HOMO to be localized*. The extent of localization appears related to the planarity of the structure, with greater planarity favoring stronger localization. Increasing the number of successively planar rings is also observed to increase localization. The importance of side chains in determining the permanent deformation is further confirmed by the strong deviation from equilibrium of the side-chain torsion angle ϕ_2 in correspondence to the HOMO localization. The presence of a structural defect in the chain when persistent localization occurs led us to suspect that the energy of the side chains maybe correlated with the localization, but no such correlation has been found. It should also be noted that, in the case of nonpersistently

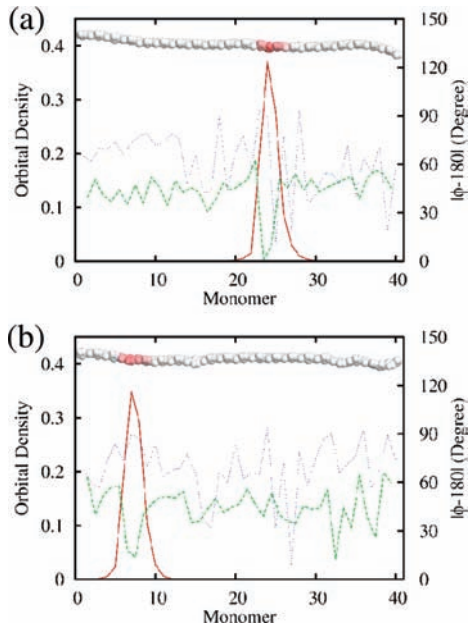

Figure 5. Relation between the inter-ring dihedral angle ϕ_1 (dashed), the ring−chain dihedral angle ϕ_2 (dotted), and the HOMO orbital density (solid line) for two strongly localized cases. In both cases ϕ_1 approaches 0° where the HOMO is localized. In case (a) a strong deviation of ϕ_2 from equilibrium is also observed.

localized states, the correlation with the planarity of the rings is poorer. We also observed that the chain deformations that support permanently localized states are never close in the chain (probably because of packing constraints), so that the concentration of these defects and the related DOS is essentially temperature independent (in agreement with the customary assumption made in device modeling[54] and implicit in the data of Table 1). The MD/QC method proposed here allows the identification of the 'hidden' disorder in the material, using experimental information for the generation of the initial packing but providing information not accessible from the experiment alone.

It is particularly important to establish what the energy of the localized states found in the simulation is and how this compares with the thermal energy. Interestingly, we found that the average energy difference between the HOMO and HOMO−1 in the case of a nonpersistently localized state is 0.046 eV, at 300 K, with a fluctuation in the energy difference of a similar magnitude (±0.031 eV) over the course of the analyzed trajectories, indicating that the energies of the traps are similar to one another; i.e. there is not a strong preference for the positive charge to occupy one of these traps and the probability of escaping from them is also relatively large. The same difference for a persistently localized HOMO is much larger (0.104 ± 0.046 eV); i.e. the static deformations which lead to persistent localization are therefore also associated with the more stable traps for the positive charge. The HOMO energy is only indicative of the relative stability of the positively charged states. These values, in fact, do not take into account the further stabilization of the localized charged state due to (i) the polarization of the surrounding environment and (ii) the relaxation of the nuclei to new equilibrium positions when a charge is present. The modification of the equilibrium position due to the extra charge is known as Holstein electron−phonon coupling in the physics literature and is the principal cause for the formation of polarons in semiconducting polymers.

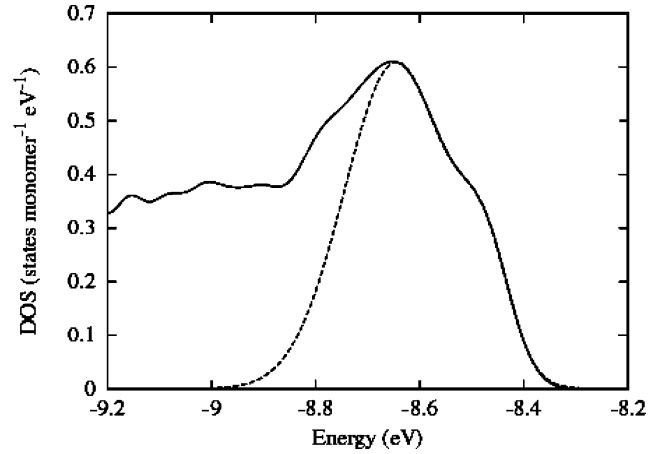

Figure 6. DOS computed with our method at 300 K (solid line) to be compared with the ones inferred from transport measurements. The dashed line, which perfectly overlaps the solid line at higher energy, is a fitting with the sum of two Gaussian functions $0.609\ \exp(-(E + 8.645)^2/2 \times 0.0995^2) + 0.192\ \exp(-(E + 8.474)^2/2 \times 0.0487^2)$.

The results of this calculation provide direct access to the density of electronic states, the most important material characteristic used to interpret the device measurements. The computed DOS (at 300 K) is reported in Figure 6, and it can be compared with the results of the many experimental evaluations (derived from fitting of the transport characteristics) provided in literature. Experimental data based on samples with good crystallinity[55] indicate that the transport measurements can be interpreted using a Gaussian DOS with broadening between 98 and 110 meV (depending on the material processing), and similar data are reported in refs 56 and 57. The band edge of our DOS can be fitted almost perfectly by the sum of two Gaussians functions (see Figure 6). The dominating function, centered on −8.645 eV, has a broadening of 99.5 meV, in very good agreement with the experimental reports. This is, to the best of our knowledge, the first evaluation of the polymer DOS from computational chemistry methods. As most of the results in organic electronics (new processing, new compounds) are discussed in terms of DOS alterations, being able to make a connection between the microscopic origin of the DOS and experiments may help the rational progress of this field. Further confirmation of our results might be possible by a more direct evaluation of the DOS.[58]

Discussion

The main result of this computational study is that the charge carriers in crystalline P3HT can be localized by static disorder. Simple inspection of the polymer conformation does not suggest the existence of energetically stable traps for the holes, and one cannot resort to the simple geometrical analysis of the polymer

(54) Pasveer, W. F.; Cottaar, J.; Tanase, C.; Coehoorn, R.; Bobbert, P. A.; Blom, P. W. M.; de Leeuw, D. M.; Michels, M. A. J. *Phys. Rev. Lett.* **2005**, *94*, 206601.
(55) Grecu, S.; Roggenbuck, A.; Opitz, A.; Brutting, W. *Org. Electron.* **2006**, *7*, 276.
(56) Tanase, C.; Meijer, E. J.; Blom, P. W. M.; de Leeuw, D. M. *Phys. Rev. Lett.* **2003**, *91*, 216601.
(57) Fumagalli, L.; Binda, M.; Natali, D.; Sampietro, M.; Salmoiraghi, E.; Di Gianvincenzo, P. *J. Appl. Phys.* **2008**, *104*, 084513.
(58) Tal, O.; Rosenwaks, Y.; Preezant, Y.; Tessler, N.; Chan, C. K.; Kahn, A. *Phys. Rev. Lett.* **2005**, *95*, 256405.

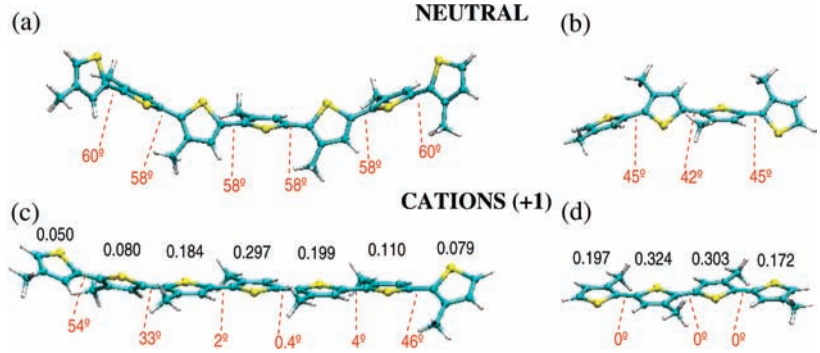

Figure 7. *Ab initio* optimized structures of hepta- and tetra-3-methylthiophene (neutral and monocation). The red figures indicate the dihedral angle between neighboring rings and the black figures indicate the total Mulliken charge on each monomer. (a) and (c) computed at the ROHF/6-31G* level; (b) and (d) computed at the MP2/6-31G* level.

to extract information on the localization length. The side chains that have been introduced to make this polymer soluble are playing an unexpectedly important role also in the electron transport: the range of different conformations accessible at room temperature causes inhomogeneities in the structure of the conjugated backbone which in turn causes permanent localization. The primary reason for trapping is therefore not the formation of a polaron (because the polaron is defined as the deformation induced by the presence of an excess charge while the deformation of this system is present *whether or not* there is an excess charge). The polaron localization length of the ideal crystalline polymer is difficult to evaluate, but it is in general predicted to be longer than six monomers;[36] i.e. the localization due to static deformations is stronger than the deformation which would be due to polaronic effects. The polaronic localization, however, is not absent, and it produces additional localization on top of the localization induced by the static disorder.

The force field used does not take into account the presence of an extra charge (because this information is not known before running the MD/QC) so the effect of nuclear and electronic relaxation around a given localized charge can only be computed in a second step. As much as it may seem appealing to build a force field which includes the effect of the extra charge on the chain, the charge dynamics (trapping, detrapping, mobility) is intrinsically a nonadiabatic (i.e., non-Born−Oppenheimer) process and cannot be captured by a purely classical model. It therefore seems that the best possible approximation is to consider the dynamics of the neutral polymer as representative of the conformations visited by the polymer at a given temperature and to include the effect of the charge on the polymer geometry as a correction.

A particularly interesting feature of P3HT localization (not necessarily valid for the general case) is that the static deformations due to structural inhomogeneities where low-energy holes are localized tend to be geometrically similar to the polaronic deformation due to the presence of an excess charge. We have performed *ab initio* optimizations of neutral and monocation hepta- and tetra-3-methylthiophene using a 6-31G* basis set and ROHF for the heptathiophene and MP2 for the tetrathiophene (ROHF results for the latter molecule are very similar). DFT was not used, as several problems are reported in the literature when this method is applied to oligothiophenes.[36,59] UHF and ROHF results are similar for both molecules, indicating that spin contamination does not affect our results.[60] As illustrated in Figure 7, while neutral hepta-3-methylthiophene shows inter-ring dihedral angles around 60° in its optimized geometry, the removal of an electron causes the planarization of a portion of four monomers in heptathiophene which carries 80% of the excess charge (also reported in Figure 7). To test that the effect was not an artifact of ROHF, we verified that a similar planarization is observed at the MP2/6-31G* level. This effect was not noted in the earlier studies of self-localization in polythiophene because the alkylic substituent (which causes the tilting of the thiophene rings) was not included in the studies and the neutral and positively charged species were both planar. The planarization is due to the fact that the HOMO orbital has an antibonding character and the removal of one electron from it will increase the tendency of the thiophene rings to lie in the same plane.

What is more important for our discussion is that the deformation that causes localization of the charge and the further deformation caused by the extra charge are very similar (local planarization in both cases), and this may explain why different experiments on P3HT have been successfully explained with apparently different theories. Optical properties have been often explained with polaron theories[61,62] (where the charge deforms the lattice), while charge transport properties are better fitted by disorder-based theories[5] (in which pre-existing disorder localizes the charge). It is also important to notice that polaronic effects alone are unable to justify the presence of localized charge in crystalline P3HT. The barrier for the hopping of a polaron (like the one depicted in Figure 7) by one monomer unit is much lower than k_BT (the value obtained from a ROHF/6-31G* calculation is 0.2 kcal/mol). Considering that the trap states due to disorder are, as we have seen, few times more stable than k_BT, we can say that the effect of static disorder is slightly more important in P3HT but polaronic effects cannot be neglected. As in any model with atomistic detail it is not straightforward to predict what characteristics of the studied material are likely to be universal for all the materials of this class. The proposed method, however, is sufficiently versatile that its application to other similar compounds should not present particular difficulties and may lead to more convenient generalizations.

Albeit it is not simple to readily adapt any of the available phenomenological models to the findings of this paper, the

(59) Choi, J.; Chipara, M.; Xu, B.; Yang, C. S.; Doudin, B.; Dowben, P. A. *Chem. Phys. Lett.* **2001**, *343*, 193.
(60) Geskin, V. M.; Cornil, J.; Bredas, J. L. *Chem. Phys. Lett.* **2005**, *403*, 228.
(61) Brown, P. J.; Sirringhaus, H.; Harrison, M.; Shkunov, M.; Friend, R. H. *Phys. Rev. B* **2001**, *6312*, 125204.
(62) Cornil, J.; Beljonne, D.; Bredas, J. L. *J. Chem. Phys.* **1995**, *103*, 842.

character of the trapped states found in here (infrequent shallow energy traps) seems to be more consistent with the multiple trapping model proposed by Salleo et al.[24] One can assume a band-like conductance in between traps and can explain the temperature dependence as due to the activated detrapping of the hole. Alternatively, in the limit of low temperature and low trap concentration one can be in the regime of 'conformationally gated transport',[63] i.e. the trapped charge will leave its localized state only when a new stable state is formed nearby by the (slow) structural fluctuation of the polymer. The computation of the microscopic rate for these processes will therefore constitute a natural continuation of this work. It has been noted, in fact, that the exact nature of the rate expression influences other important macroscopic parameters such as the electric field dependence of the charge mobility.[64]

In conclusion, we have shown in this contribution that it is possible to compute the electronic structure of the charge carrier in a realistic polymer without any *a priori* assumption on the nature of charge transport. Using a versatile combination of molecular dynamics simulation and quantum chemical methods one can add a detailed microscopic picture to the statistical methods used to describe transport in polymers. This detailed description is in turn essential to developing an understanding of the relation between chemical structure and charge mobility in polymers.

Acknowledgment. This work was supported by EPSRC (UK). We are very grateful to Nir Tessler (Technion), Alberto Salleo (Stanford) and Henning Sirringhaus (Cambridge) for important comments and suggestions regarding this work.

Supporting Information Available: This material is available free of charge via the Internet at http://pubs.acs.org.

JA903843C

(63) Berlin, Y. A.; Burin, A. L.; Siebbeles, L. D. A.; Ratner, M. A. *J. Phys. Chem. A* **2001**, *105*, 5666.

(64) Preezant, Y.; Tessler, N. *Phys. Rev. B* **2006**, *74*, 235202.